Letter

Effect of magnetism and phonons on localized carriers in the ferrimagnetic kagome metals $GdMn_6Sn_6$ and $TbMn_6Sn_6$

M. Wenzel,[1,*] A. A. Tsirlin,[2,3] O. Iakutkina,[1] Q. Yin,[4] H. C. Lei,[4] M. Dressel,[1] and E. Uykur[1,5]

[1]*1. Physikalisches Institut, Universität Stuttgart, 70569 Stuttgart, Germany*

[2]*Felix Bloch Institute for Solid-State Physics, Leipzig University, 04103 Leipzig, Germany*

[3]*Experimental Physics VI, Center for Electronic Correlations and Magnetism, Institute of Physics, University of Augsburg, 86135 Augsburg, Germany*

[4]*Laboratory for Neutron Scattering, and Beijing Key Laboratory of Optoelectronic Functional Materials MicroNano Devices, Department of Physics, Renmin University of China, Beijing 100872, China*

[5]*Helmholtz-Zentrum Dresden-Rossendorf, Institute of Ion Beam Physics and Materials Research, 01328 Dresden, Germany*

(Received 31 July 2022; accepted 1 December 2022; published 19 December 2022)

Kagome metals possess peculiar optical spectra consisting of contributions from free charge carriers in a Drude-type response, localized carriers seen as a strongly temperature-dependent localization peak, and, in some cases, phonons displaying strong anomalies. The rare-earth kagome metal series, RMn_6Sn_6, provides a marvelous playground to study the electronic properties of kagome metals in the presence of variable magnetic order. Here, we report temperature-dependent reflectivity studies on two members of the RMn_6Sn_6 family, $GdMn_6Sn_6$ (in-plane ferrimagnet) and $TbMn_6Sn_6$ (out-of-plane ferrimagnet), in a broad energy range (50–18 000 cm^{-1}, equivalent to 6.2 meV–2.23 eV) down to 10 K. At high temperatures, a phonon mode at approximately 160 cm^{-1} is observed, which becomes screened out in $TbMn_6Sn_6$ below ∼150 K as the localization peak linearly passes through the mode. In $GdMn_6Sn_6$, the disappearance of the phonon is accompanied by the onset of saturation of the peak position, suggesting an unusual interplay between the two features.

DOI: 10.1103/PhysRevB.106.L241108

Proposed by Syôzi in 1951, the kagome lattice quickly became popular among both theoretical and experimental physicists due to its unique magnetic and electronic properties [1,2]. Consisting of spatially separated metallic kagome planes, kagome metals are model compounds for studying strong electronic correlations, magnetism, and topologically nontrivial states [3]. Here, the itinerant carriers give rise to the peculiar kagome electronic band structure hosting dispersionless flat bands, saddle points, as well as linearly dispersing Dirac bands [4–9].

The ternary rare-earth series, RMn_6Sn_6 (R = Sc, Y, Gd-Lu), opens new ways to investigate the influence of magnetism on the electronic properties of kagome metals, and hence distinguish between magnetic-driven and kagome layer-driven properties. While these compounds have been studied extensively over the last three decades regarding their unusual magnetic structure, they recently gained attention in the framework of kagome metals [10–12]. These compounds crystallize in the $P6/mmm$ space group featuring spatially decoupled magnetic Mn-kagome planes stacked along the c axis, which are stabilized by Sn1 atoms. Within one unit cell, the kagome layers are separated by nonmagnetic Sn2 atoms forming a honeycomb lattice, while RSn3 layers separate the kagome planes from one unit cell to another, as sketched in Figs. 1(a) and 1(b). The underlying magnetic structure strongly depends on the rare-earth element separating the layers, resulting in a large variety of ferrimagnetic (R = Gd, Tb, Dy, Ho) and antiferromagnetic (R = Sc, Y, Er, Tm, Yb, Lu) ground states across the series [10,13].

Angle-resolved photoemission spectroscopy (ARPES) and Landau level measurements reveal the signatures of the kagome lattice, including topologically nontrivial Dirac bands and flat bands in these materials [7,9,12,14]. Comprising spin-polarized Mn 3d states with a strong intrinsic spin-orbit coupling, these two-dimensional kagome bands exhibit nontrivial Chern numbers [6,7,15] giving rise to an intrinsic anomalous Hall effect [16–21]. While the different magnetic structures do not seem to affect the main band dispersions near the Fermi energy E_F, significantly, a gap at the Dirac points has been proposed only for the ferrimagnetic systems [12,22–24]. Moreover, this Chern gap, as well as the energy of the Dirac points E_D, can be tuned with the rare-earth element [22]. Here, the number of unpaired 4f electrons of the rare-earth element plays an important role as a coupling between the 4f and the 3d electrons is observed.

The key implications of these topological features lie in unusual transport properties that crucially rely on charge carriers and their dynamics [12,27–29]. Especially, the effect of magnetism is one of the central issues [30]. Therefore, here, we study these dynamics and their dependence on the magnetic order with temperature-dependent broadband Fourier transform infrared spectroscopy studies on RMn_6Sn_6 systems, namely on $GdMn_6Sn_6$ and $TbMn_6Sn_6$. While both systems possess an almost identical crystal structure and a ferrimagnetic ground state below room temperature, in the

*maxim.wenzel@pi1.physik.uni-stuttgart.de

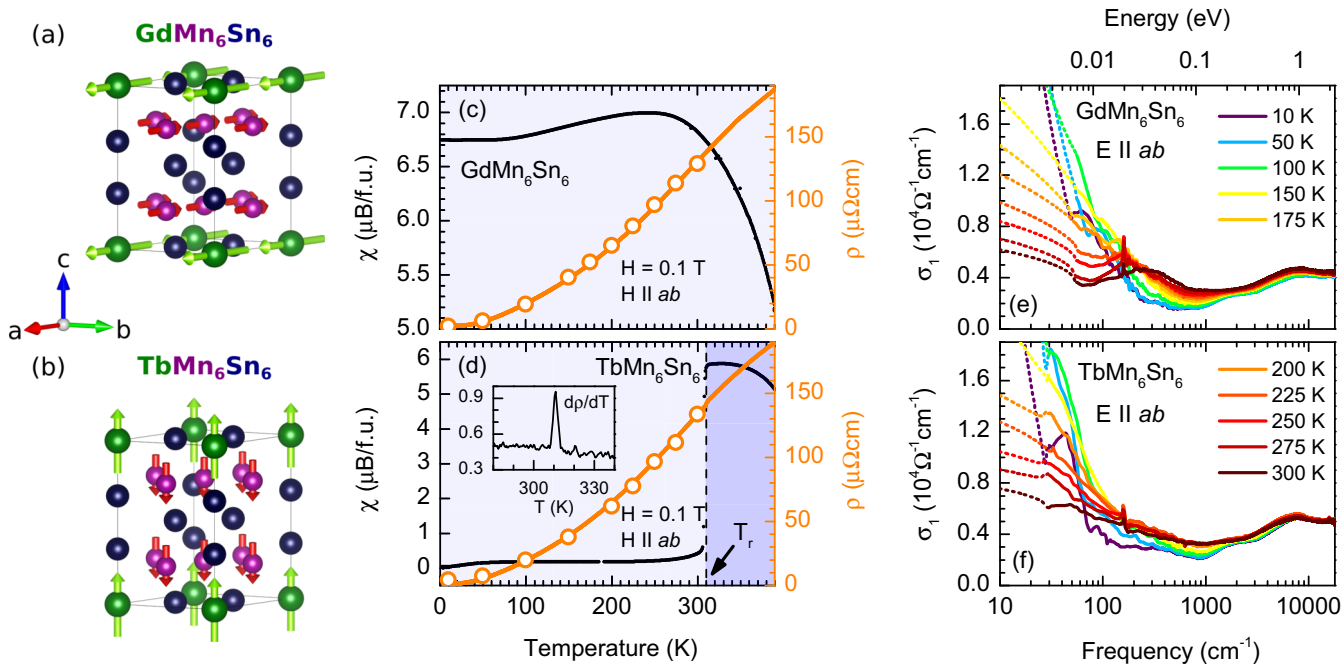

FIG. 1. (a) and (b) Crystal and magnetic structure below 300 K of $GdMn_6Sn_6$ and $TbMn_6Sn_6$, respectively [13,25]. (c) and (d) Magnetic susceptibility and dc resistivity curves measured in the *ab* plane. The Curie temperature of both systems lies above the measured temperature range; however, a spin reorientation from the basal plane near to the *c* axis around $T_r \sim 310$ K is visible for $TbMn_6Sn_6$. For $GdMn_6Sn_6$, no anomalies are observed in the measured temperature range. Open circles are the dc resistivity values obtained from the Hagen-Rubens fits of the optical measurements as explained in the Supplemental Material [26]. (e) and (f) Temperature-dependent in-plane optical conductivity with the dotted lines being the Hagen-Rubens extrapolation to low energies.

former one, the spins are aligned within the kagome plane, whereas in the Tb compound, a perpendicular alignment to the kagome layers is reported [10,13,31–33]. This was confirmed prior to our optical study by dc transport and magnetic susceptibility measurements shown in Figs. 1(c) and 1(d). We further performed density functional theory plus Hubbard U (DFT+U) calculations to evaluate the electronic structures, revealing the correlated character of the RMn_6Sn_6 series. Due to localization effects, the optical response of the charge carriers splits into the conventional Drude part and a prominent low-energy peak. This peak shows a clear dependence on the magnetic order and underlies the magnetic tunability of this compound family.

Figures 1(e) and 1(f) display the temperature-dependent real part of the in-plane optical conductivity of $GdMn_6Sn_6$ and $TbMn_6Sn_6$, respectively. At first glance, the spectra are remarkably similar and resemble the spectrum of the ferromagnetic Fe_3Sn_2 [34,35]. Consistent with the metallic nature of these compounds, a very narrow Drude component is observed at low energies, which becomes even sharper upon cooling. For $GdMn_6Sn_6$, only the tail of this feature is visible even at 300 K. Two steplike absorption features can be identified in the otherwise relatively flat conductivity at high energies. Very similar steps were interpreted as the signature of two-dimensional Dirac fermions in Fe_3Sn_2. In addition to the sharp Drude component and interband transitions, a phonon mode around 160 cm^{-1} is observed. Furthermore, we have realized that the low-energy dynamics cannot be reproduced only with a single Drude component, but an additional peaklike absorption feature is required as shown in Figs. 2(a) and 2(b) for the data at 300 K. With this peak showing a strong redshift upon cooling, it puts the RMn_6Sn_6 series on common ground with other kagome metals and clearly separates this feature from other low-energy transitions, which are interband in nature [34,36–38].

A closer look at the low-energy regime reveals substantial differences between the two ferrimagnetic compounds. Figures 2(b) and 2(d) show the temperature evolution of this so-called localization peak in $GdMn_6Sn_6$ and $TbMn_6Sn_6$ after subtracting the fitted Drude, phonon, and interband contributions from the experimental optical conductivity. Not only is the localization peak more pronounced in the in-plane ferrimagnetic system $GdMn_6Sn_6$, but the peak position saturates at low temperatures, as shown in Fig. 2(a). In contrast, a linear redshift over the whole temperature range is observed in $TbMn_6Sn_6$ [see Fig. 2(c)]. Hence, the peak moves out of the measured range at low temperatures, and its position has to be estimated from its high-frequency tail, as well as by considering the linear behavior of the shift at higher temperatures, leading to increasing error bars of the fits.

Visually, the temperature evolution of the peak position in $GdMn_6Sn_6$ looks strikingly similar to the behavior in Fe_3Sn_2. For the latter, a possible coupling between the localization peak and the underlying magnetic structure is discussed since the linear scaling breaks down after a reorientation of the Fe spins at 120 K [34,39]. Additionally, the shape of the peak transforms into a sharp Fano resonance. The saturation as observed in $GdMn_6Sn_6$ was also reported in the nonmagnetic

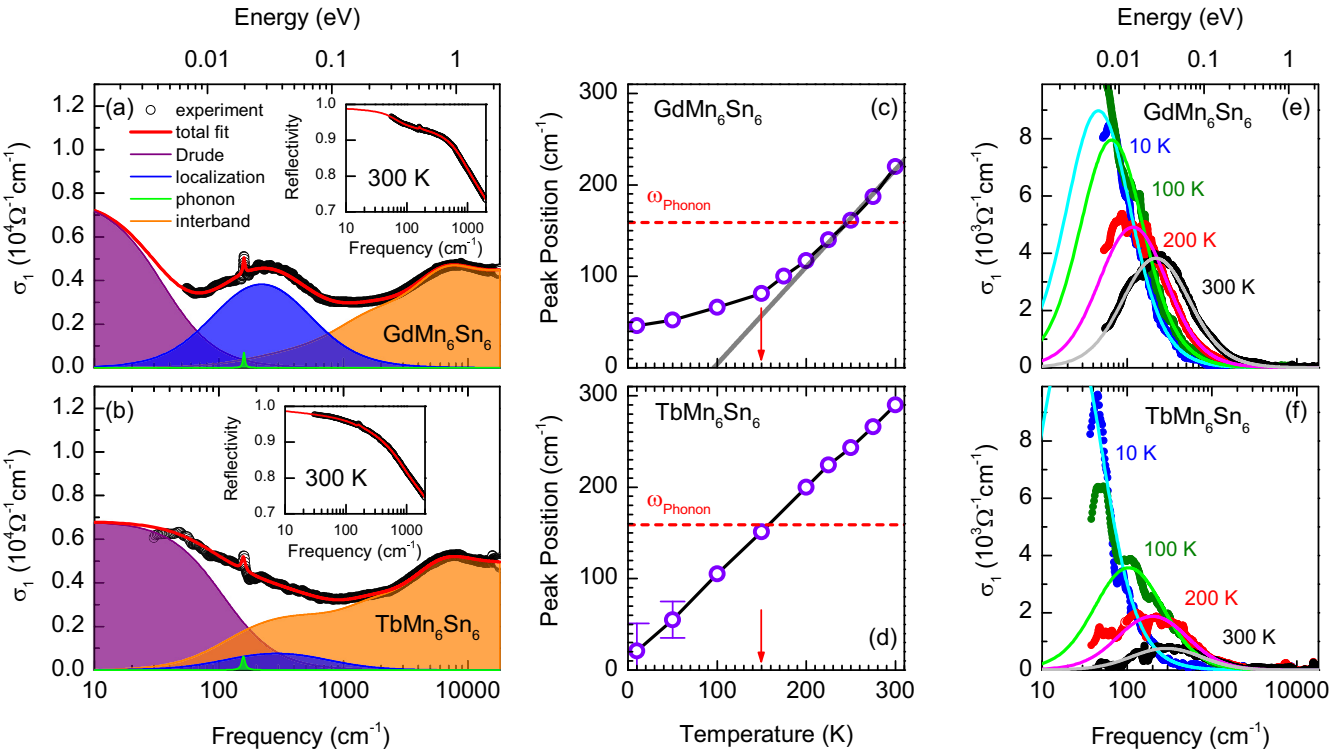

FIG. 2. (a) and (b) Decomposed optical conductivity at 300 K, consisting of a Drude component (purple), a localization peak (blue), a phonon mode (green), and several interband transitions (orange). The insets show the total fit to the measured reflectivity. Details on the fitting process as well as the decomposed spectra at lower temperatures can be found in the Supplemental Material [26]. (c) and (d) Temperature dependence of the localization peak position. The red dashed line marks the phonon mode, while the red arrow indicates the temperature where the mode disappears. (e) and (f) Temperature evolution of the localization peak, obtained by subtracting the fitted Drude, phonon mode, and interband contributions from the spectra. The solid lines are the Fratini model fits to the total experimental conductivity as described in the Supplemental Material [26].

KV_3Sb_5, suggesting that the origin of this effect may be other than magnetic. Additionally, no change of the in-plane ferrimagnetic structure of $GdMn_6Sn_6$ is reported below room temperature; hence, the primary cause for the observed saturation must be something else. Nevertheless, a commonality between the two magnetic systems is the in-plane direction of the magnetic moments in both Fe_3Sn_2 below its spin-reorientation transition and $GdMn_6Sn_6$.

One plausible explanation for the observed saturation uniting magnetic and nonmagnetic kagome metals is the involvement of a phonon mode. Indeed, phonons and their importance for the electronic structure of kagome metals have been studied in multiple compounds. In the AV_3Sb_5 family, phonons are discussed to be the driving force behind the charge-density-wave formation and the low-temperature superconductivity [40,41]. Optical measurements revealed strong phonon anomalies associated with a coupling of the phonon modes to the electronic background in KV_3Sb_5 and RbV_3Sb_5 [36,37]. Furthermore, a strong interplay between phonons and fermionic degrees of freedom was revealed by scanning tunneling microscopy (STM) studies of paramagnetic CoSn [42].

DFT calculations, shown in the Supplemental Material [26], reveal a total number of nine IR-active phonon modes in each compound. Four of these modes have the A_{2u} symmetry involving out-of-plane atomic displacements and hence cannot be detected by our in-plane measurements. While in highly metallic systems phonon modes are often too weak to be detected and/or screened by the free carriers, our measurements were able to capture a prominent E_{1u} mode around 160 cm^{-1} at room temperature. At low temperatures, this mode disappears in both compounds. At first glance, this anomalous behavior might be explained by a structural distortion; however, low-temperature XRD studies report almost no changes in the crystal structure of RMn_6Sn_6 down to 2 K [13,25]. Hence, an interplay between the phonon mode and the localization peak has to be considered as a possible scenario, not least because both features are located around the same energy range.

For a further comparison of the two features, the position of the phonon mode is marked with the red dashed line in Figs. 2(a) and 2(c), while the red arrow points at the temperature at which the phonon mode disappears in each compound. In $TbMn_6Sn_6$, the phonon mode disappears as soon as the localization peak passes through it, suggesting that the localization peak screens out the phonon mode. On the other hand, a more complex relationship between the two features is observed in $GdMn_6Sn_6$. Here, the phonon mode shows an enhancement and a slight broadening as the localization peak passes through it, and is retained even below the crossing over a narrow temperature range. Eventually, the mode disappears around the temperature where the position of

the localization peak saturates. This behavior suggests an unusual coupling between the phonon mode and the localization peak in $GdMn_6Sn_6$. Based on the observation that the strong localization peak anomalies appear in the in-plane ferromagnetic system, one plausible explanation would be a magnetoelastic coupling to the in-plane infrared-active phonon mode. Additionally, the rare-earth element could directly influence the phonon mode and hence its interplay with the localization peak.

Ultimately, an interplay with some other bosonic excitations such as magnons, for instance, could as well lead to the distinct behavior of the localization peak in $GdMn_6Sn_6$ compared to $TbMn_6Sn_6$. Indeed, magnon bands extending to energies up to ∼100 meV have been reported in several members of the RMn_6Sn_6 family [43,44].

The presence of a redshifting localization peak is a common occurrence in systems with slow electron dynamics, such as organic conductors, cuprates, and manganites [45,46], many of them being strongly correlated materials. Hence, we now turn to analyzing the electronic correlations in the RMn_6Sn_6 series. Figures 3(a) and 3(b) show the comparison between the experimental and the calculated optical conductivities using DFT taking into account the different magnetic structures. For all calculations, a Hubbard $U_R = 10$ eV was added to the rare-earth element with the DFT+U method using the double-counting correction in the fully localized limit to treat the strongly correlated $4f$ electrons [9,47–49]. In the case of $GdMn_6Sn_6$, a good agreement with the experiment is found, while for $TbMn_6Sn_6$, the low-energy spectral weight cannot be reproduced with this method. The agreement is improved by adding a Hubbard $U_{\mathrm{Mn}} = 0.4$ eV to the Mn atoms. Another possibility is shifting the Fermi energy down by 47 meV; however, this requires removing one electron from the structure, which is hard to reconcile with the system.

Although with different adjustments, one can bring the calculations to the experiment's level, in either case, the energy of the calculated conductivity needs to be rescaled by a factor of 2.5 in $GdMn_6Sn_6$ (2 in $TbMn_6Sn_6$). A very similar scaling factor was previously reported for ARPES measurements of $GdMn_6Sn_6$ [9]. This suggests that these systems are clearly beyond DFT, and electronic correlations therein cannot be fully treated on the mean-field DFT+U level.

We further observed the steplike absorption features, combined with the relatively flat optical conductivity, as the potential signatures of the Dirac points in these systems. Considering that there are two Dirac points, one above and one below the Fermi energy (see Supplemental Material [26]), one would expect these steplike absorption features to appear [34]. This interpretation becomes even more tempting when the energies of the steps are compared with the ARPES measurements. However, considering the relatively high energy range of these features and the significant number of bands crossing the Fermi energy, the step-like absorption is most likely just a cumulative effect of different contributions; hence, one should be careful in its assignment. On the other hand, absorption features at lower energies ($\omega < 1000$ cm^{-1}) can be related to transitions between bands very close to the Fermi energy, most probably involving transitions between the saddle points nearby the M point, as shown in our band-structure calculations in the Supplemental Material [26].

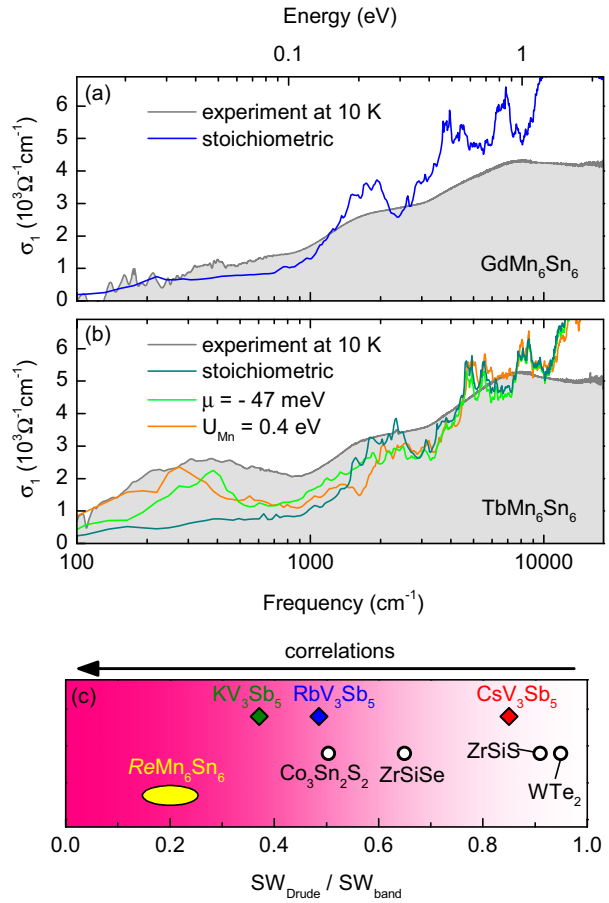

FIG. 3. (a) and (b) Experimental interband transitions along with the DFT+U calculated optical conductivity. For all calculations a Hubbard $U_R = 10$ eV was added to the rare-earth element. Furthermore, the energy scale of the calculated conductivity is rescaled for a better comparison with the experiment. (c) Correlation scaling for different kagome metals and other topological materials taken from Ref. [50].

Although the RMn_6Sn_6 series lies beyond the limits of the DFT+U methods presented here, the calculations can be used for an initial assessment of the correlation strength. As proposed previously for different compounds, including cuprates, iron pnictides, and topologically nontrivial Dirac systems [50,51], the ratio of the spectral weight of the mobile carriers from the experiment and the DFT calculations can be used as a gauge of electronic correlations. Here, $\mathrm{SW_{Drude}}/\mathrm{SW_{band}}$ is close to 1 for uncorrelated materials, while the ratio becomes zero for Mott insulators showing the most correlated behavior. Figure 3(c) depicts this scaling for the AV_3Sb_5 series and topological semimetals taken from Refs. [36,50]. From the calculations, we can determine a rough value of $\mathrm{SW_{Drude}}/\mathrm{SW_{band}} \approx 0.2$, pointing towards much stronger correlations in comparison with the AV_3Sb_5 series and other kagome metals reported to date. Moreover, no significant difference between $GdMn_6Sn_6$ and $TbMn_6Sn_6$ is observed, whereas the correlation strength changes drastically between different members of the AV_3Sb_5 family.

In summary, we establish the correlated nature of ferrimagnetic kagome metals of the RMn_6Sn_6 family and uncover

partial localization of charge carriers manifested by the prominent low-energy peak in the optical conductivity. The temperature evolution of this peak is sensitive to details of the magnetic order. While in $TbMn_6Sn_6$, the localization peak redshifts linearly through the whole temperature range upon cooling and screens out the phonon mode at $\sim$160 cm^{-1}, it displays different characteristics in $GdMn_6Sn_6$. Here, the peak is more pronounced, while its position saturates at low temperatures. This dissimilar behavior indicates a major difference in low-energy degrees of freedom that damp electron dynamics and, consequently, should affect transport properties at low temperatures. Both compounds display a strongly correlated character, as a good agreement with the experimental interband transitions is only found after rescaling the energy of the calculated optical conductivity, and the experimental Drude spectral weight is drastically lower than the DFT prediction.

The authors acknowledge the fruitful discussion with Simone Fratini, and technical support by Gabriele Untereiner. We also thank Falk Lissner and Rainer Niewa for the XRD measurements. H.C.L. was supported by National Key R&D Program of China (Grant No. 2018YFE0202600), the Beijing Natural Science Foundation (Grant No. Z200005), the Fundamental Research Funds for the Central Universities and Research Funds of Renmin University of China (RUC) (Grants No. 18XNLG14, No. 19XNLG13, and No. 19XNLG17), and the Beijing National Laboratory for Condensed Matter Physics. The work has been supported by the Deutsche Forschungsgemeinschaft (DFG) via Grants No. UY63/2-1, No. DR228/48-1, and No. DR228/51-1. E.U. acknowledges the European Social Fund and the Baden-Württemberg Stiftung for the financial support of this research project by the Eliteprogramme.

[1] I. Syôzi, Statistics of kagomé lattice, Prog. Theor. Phys. **6**, 306 (1951).

[2] M. Mekata, Kagome: The story of the basketweave lattice, Phys. Today **56**(2), 12 (2003).

[3] D. F. Liu, A. J. Liang, E. K. Liu, Q. N. Xu, Y. W. Li, C. Chen, D. Pei, W. J. Shi, S. K. Mo, P. Dudin, T. Kim, C. Cacho, G. Li, Y. Sun, L. X. Yang, Z. K. Liu, S. S. P. Parkin, C. Felser, and Y. L. Chen, Magnetic Weyl semimetal phase in a kagomé crystal, Science **365**, 1282 (2019).

[4] W.-S. Wang, Z.-Z. Li, Y.-Y. Xiang, and Q.-H. Wang, Competing electronic orders on kagome lattices at van Hove filling, Phys. Rev. B **87**, 115135 (2013).

[5] Z. Lin, J.-H. Choi, Q. Zhang, W. Qin, S. Yi, P. Wang, L. Li, Y. Wang, H. Zhang, Z. Sun, L. Wei, S. Zhang, T. Guo, Q. Lu, J.-H. Cho, C. Zeng, and Z. Zhang, Flatbands and Emergent Ferromagnetic Ordering in Fe_3Sn_2 Kagome Lattices, Phys. Rev. Lett. **121**, 096401 (2018).

[6] M. Kang, L. Ye, S. Fang, J.-S. You, A. Levitan, M. Han, J. I. Facio, C. Jozwiak, A. Bostwick, E. Rotenberg, M. K. Chan, R. D. McDonald, D. Graf, K. Kaznatcheev, E. Vescovo, D. C. Bell, E. Kaxiras, J. van den Brink, M. Richter, M. Prasad Ghimire *et al.*, Dirac fermions and flat bands in the ideal kagome metal FeSn, Nat. Mater. **19**, 163 (2020).

[7] M. Li, Q. Wang, G. Wang, Z. Yuan, W. Song, R. Lou, Z. Liu, Y. Huang, Z. Liu, H. Lei, Z. Yin, and S. Wang, Dirac cone, flat band and saddle point in kagome magnet YMn_6Sn_6, Nat. Commun. **12**, 3129 (2021).

[8] Z. Liu, M. Li, Q. Wang, G. Wang, C. Wen, K. Jiang, X. Lu, S. Yan, Y. Huang, D. Shen, J.-X. Yin, Z. Wang, Z. Yin, H. Lei, and S. Wang, Orbital-selective Dirac fermions and extremely flat bands in frustrated kagome-lattice metal CoSn, Nat. Commun. **11**, 4002 (2020).

[9] Z. Liu, N. Zhao, M. Li, Q. Yin, Q. Wang, Z. Liu, D. Shen, Y. Huang, H. Lei, K. Liu, and S. Wang, Electronic correlation effects in the kagome magnet $GdMn_6Sn_6$, Phys. Rev. B **104**, 115122 (2021).

[10] G. Venturini, B. Chafik El Idrissi, and B. Malaman, Magnetic properties of RMn_6Sn_6 (R = Sc, Y, Gd-Tm, Lu) compounds with $HfFe_6Ge_6$ type structure, J. Magn. Magn. Mater. **94**, 35 (1991).

[11] N. J. Ghimire, R. L. Dally, L. Poudel, D. C. Jones, D. Michel, N. T. Magar, M. Bleuel, M. A. McGuire, J. S. Jiang, J. F. Mitchell, J. W. Lynn, and I. I. Mazin, Competing magnetic phases and fluctuation-driven scalar spin chirality in the kagome metal YMn_6Sn_6, Sci. Adv. **6**, eabe2680 (2020).

[12] J.-X. Yin, W. Ma, T. A. Cochran, X. Xu, S. S. Zhang, H.-J. Tien, N. Shumiya, G. Cheng, K. Jiang, B. Lian, Z. Song, G. Chang, I. Belopolski, D. Multer, M. Litskevich, Z.-J. Cheng, X. P. Yang, B. Swidler, H. Zhou, H. Lin *et al.*, Quantum-limit Chern topological magnetism in $TbMn_6Sn_6$, Nature (London) **583**, 533 (2020).

[13] B. Malaman, G. Venturini, R. Welter, J. Sanchez, P. Vulliet, and E. Ressouche, Magnetic properties of RMn_6Sn_6 (R=Gd-Er) compounds from neutron diffraction and Mössbauer measurements, J. Magn. Magn. Mater. **202**, 519 (1999).

[14] X. Gu, C. Chen, W. S. Wei, L. L. Gao, J. Y. Liu, X. Du, D. Pei, J. S. Zhou, R. Z. Xu, Z. X. Yin, W. X. Zhao, Y. D. Li, C. Jozwiak, A. Bostwick, E. Rotenberg, D. Backes, L. S. I. Veiga, S. Dhesi, T. Hesjedal, G. van der Laan *et al.*, Robust kagome electronic structure in the topological quantum magnets XMn_6Sn_6 (X = Dy, Tb, Gd, Y), Phys. Rev. B **105**, 155108 (2022).

[15] G. Xu, B. Lian, and S.-C. Zhang, Intrinsic Quantum Anomalous Hall Effect in the Kagome Lattice $Cs_2LiMn_3F_{12}$, Phys. Rev. Lett. **115**, 186802 (2015).

[16] W. Ma, X. Xu, Z. Wang, H. Zhou, M. Marshall, Z. Qu, W. Xie, and S. Jia, Anomalous Hall effect in the distorted kagome magnets (Nd,Sm)Mn_6Sn_6, Phys. Rev. B **103**, 235109 (2021).

[17] C. Q. Xu, T. W. Heitmann, H. Zhang, X. Xu, and X. Ke, Magnetic phase transition, magnetoresistance, and anomalous Hall effect in Ga-substituted YMn_6Sn_6 with a ferromagnetic kagome lattice, Phys. Rev. B **104**, 024413 (2021).

[18] X. Xu, J.-X. Yin, W. Ma, H.-J. Tien, X.-B. Qiang, P. V. S. Reddy, H. Zhou, J. Shen, H.-Z. Lu, T.-R. Chang, Z. Qu, and S. Jia, Topological charge-entropy scaling in kagome Chern magnet $TbMn_6Sn_6$, Nat. Commun. **13**, 1197 (2022).

[19] L. Gao, S. Shen, Q. Wang, W. Shi, Y. Zhao, C. Li, W. Cao, C. Pei, J.-Y. Ge, G. Li, J. Li, Y. Chen, S. Yan, and Y. Qi, Anomalous Hall effect in ferrimagnetic metal RMn_6Sn_6 (R = Tb, Dy, Ho) with clean Mn kagome lattice, Appl. Phys. Lett. **119**, 092405 (2021).

[20] T. Asaba, S. M. Thomas, M. Curtis, J. D. Thompson, E. D. Bauer, and F. Ronning, Anomalous Hall effect in the kagome ferrimagnet $GdMn_6Sn_6$, Phys. Rev. B **101**, 174415 (2020).

[21] G. Dhakal, F. Cheenicode Kabeer, A. K. Pathak, F. Kabir, N. Poudel, R. Filippone, J. Casey, A. Pradhan Sakhya, S. Regmi, C. Sims, K. Dimitri, P. Manfrinetti, K. Gofryk, P. M. Oppeneer, and M. Neupane, Anisotropically large anomalous and topological Hall effect in a kagome magnet, Phys. Rev. B **104**, L161115 (2021).

[22] W. Ma, X. Xu, J.-X. Yin, H. Yang, H. Zhou, Z.-J. Cheng, Y. Huang, Z. Qu, F. Wang, M. Z. Hasan, and S. Jia, Rare Earth Engineering in RMn_6Sn_6 (R = Gd−Tm, Lu) Topological Kagome Magnets, Phys. Rev. Lett. **126**, 246602 (2021).

[23] F. D. M. Haldane, Model for a Quantum Hall Effect without Landau Levels: Condensed-Matter Realization of the "Parity Anomaly", Phys. Rev. Lett. **61**, 2015 (1988).

[24] C. Sims, Existence of Chern Gaps in Kagome Magnets RMn_6Ge_6 (R = Nd, Sm, Tb, Dy, Ho, Er, Yb, Lu), arXiv:2203.09447.

[25] B. El Idrissi, G. Venturini, B. Malaman, and D. Fruchart, Magnetic structures of $TbMn_6Sn_6$ and $HoMn_6Sn_6$ compounds from neutron diffraction study, J. Less-Common Met. **175**, 143 (1991).

[26] See Supplemental Material at http://link.aps.org/supplemental/10.1103/PhysRevB.106.L241108 for experimental details, extended data analysis, and details on phonon and band structure calculations, which includes Refs. [52–61].

[27] B. R. Ortiz, L. C. Gomes, J. R. Morey, M. Winiarski, M. Bordelon, J. S. Mangum, I. W. H. Oswald, J. A. Rodriguez-Rivera, J. R. Neilson, S. D. Wilson, E. Ertekin, T. M. McQueen, and E. S. Toberer, New kagome prototype materials: Discovery of KV_3Sb_5, RbV_3Sb_5, and CsV_3Sb_5, Phys. Rev. Mater. **3**, 094407 (2019).

[28] T. Neupert, M. M. Denner, J.-X. Yin, R. Thomale, and M. Z. Hasan, Charge order and superconductivity in kagome materials, Nat. Phys. **18**, 137 (2022).

[29] H. Zhang, J. Koo, C. Xu, M. Sretenovic, B. Yan, and X. Ke, Exchange-biased topological transverse thermoelectric effects in a Kagome ferrimagnet, Nat. Commun. **13**, 1091 (2022).

[30] Z.-J. Cheng, I. Belopolski, T. A. Cochran, H.-J. Tien, X. P. Yang, W. Ma, J.-X. Yin, J. Zhang, C. Jozwiak, A. Bostwick, E. Rotenberg, G. Cheng, M. S. Hossain, Q. Zhang, N. Shumiya, D. Multer, M. Litskevich, Y. Jiang, N. Yao, B. Lian *et al.*, Magnetization-direction-tunable kagome Weyl line, arXiv:2203.10648.

[31] S. Tabatabai Yazdi, N. Tajabor, M. Behdani, M. Rezaee Roknabadi, D. Sanavi Khoshnoud, and F. Pourarian, Magnetoelastic properties of $GdMn_6Sn_6$ intermetallic compound, J. Magn. Magn. Mater. **323**, 2070 (2011).

[32] D. C. Jones, S. Das, H. Bhandari, X. Liu, P. Siegfried, M. P. Ghimire, S. S. Tsirkin, I. I. Mazin, and N. J. Ghimire, Origin of spin reorientation and intrinsic anomalous Hall effect in the kagome ferrimagnet $TbMn_6Sn_6$, arXiv:2203.17246.

[33] C. Mielke III, W. L. Ma, V. Pomjakushin, O. Zaharko, S. Sturniolo, X. Liu, V. Ukleev, J. S. White, J.-X. Yin, S. S. Tsirkin, C. B. Larsen, T. A. Cochran, M. Medarde, V. Porée, D. Das, R. Gupta, C. N. Wang, J. Chang, Z. Q. Wang, R. Khasanov *et al.*, Low-temperature magnetic crossover in the topological kagome magnet $TbMn_6Sn_6$, Commun. Phys. **5**, 107 (2022).

[34] A. Biswas, O. Iakutkina, Q. Wang, H. C. Lei, M. Dressel, and E. Uykur, Spin-Reorientation-Induced Band Gap in Fe_3Sn_2: Optical Signatures of Weyl Nodes, Phys. Rev. Lett. **125**, 076403 (2020).

[35] F. Schilberth, N. Unglert, L. Prodan, F. Meggle, J. Ebad Allah, C. A. Kuntscher, A. A. Tsirlin, V. Tsurkan, J. Deisenhofer, L. Chioncel, I. Kézsmárki, and S. Bordács, Magneto-optical detection of topological contributions to the anomalous Hall effect in a kagome ferromagnet, Phys. Rev. B **106**, 144404 (2022).

[36] M. Wenzel, B. R. Ortiz, S. D. Wilson, M. Dressel, A. A. Tsirlin, and E. Uykur, Optical study of RbV_3Sb_5: Multiple density-wave gaps and phonon anomalies, Phys. Rev. B **105**, 245123 (2022).

[37] E. Uykur, B. R. Ortiz, S. D. Wilson, M. Dressel, and A. A. Tsirlin, Optical detection of the density-wave instability in the kagome metal KV_3Sb_5, npj Quantum Mater. **7**, 16 (2022).

[38] E. Uykur, B. R. Ortiz, O. Iakutkina, M. Wenzel, S. D. Wilson, M. Dressel, and A. A. Tsirlin, Low-energy optical properties of the nonmagnetic kagome metal CsV_3Sb_5, Phys. Rev. B **104**, 045130 (2021).

[39] N. Kumar, Y. Soh, Y. Wang, and Y. Xiong, Magnetotransport as a diagnostic of spin reorientation: Kagome ferromagnet as a case study, Phys. Rev. B **100**, 214420 (2019).

[40] H. Luo, Q. Gao, H. Liu, Y. Gu, D. Wu, C. Yi, J. Jia, S. Wu, X. Luo, Y. Xu, L. Zhao, Q. Wang, H. Mao, G. Liu, Z. Zhu, Y. Shi, K. Jiang, J. Hu, Z. Xu, and X. J. Zhou, Electronic nature of charge density wave and electron-phonon coupling in kagome superconductor KV_3Sb_5, Nat. Commun. **13**, 273 (2022).

[41] Y. Zhong, S. Li, H. Liu, Y. Dong, Y. Arai, H. Li, Y. Shi, Z. Wang, S. Shin, H. N. Lee, H. Miao, T. Kondo, and K. Okazaki, Testing electron-phonon coupling for the superconductivity in kagome metal CsV_3Sb_5, arXiv:2207.02407.

[42] J.-X. Yin, N. Shumiya, S. Mardanya, Q. Wang, S. S. Zhang, H.-J. Tien, D. Multer, Y. Jiang, G. Cheng, N. Yao, S. Wu, D. Wu, L. Deng, Z. Ye, R. He, G. Chang, Z. Liu, K. Jiang, Z. Wang, T. Neupert *et al.*, Fermion-boson many-body interplay in a frustrated kagome paramagnet, Nat. Commun. **11**, 4003 (2020).

[43] S. X. M. Riberolles, T. J. Slade, D. L. Abernathy, G. E. Granroth, B. Li, Y. Lee, P. C. Canfield, B. G. Ueland, L. Ke, and R. J. McQueeney, Low-Temperature Competing Magnetic Energy Scales in the Topological Ferrimagnet $TbMn_6Sn_6$, Phys. Rev. X **12**, 021043 (2022).

[44] H. Zhang, X. Feng, T. Heitmann, A. I. Kolesnikov, M. B. Stone, Y.-M. Lu, and X. Ke, Topological magnon bands in a room-temperature kagome magnet, Phys. Rev. B **101**, 100405(R) (2020).

[45] S. Fratini and S. Ciuchi, Displaced Drude peak and bad metal from the interaction with slow fluctuations, SciPost Phys. **11**, 039 (2021).

[46] L. V. Delacrétaz, B. Goutéraux, S. A. Hartnoll, and A. Karlsson, Bad metals from fluctuating density waves, SciPost Phys. **3**, 025 (2017).

[47] M. Petersen, J. Hafner, and M. Marsman, Structural, electronic and magnetic properties of Gd investigated by DFT+U

methods: bulk, clean and H-covered (0001) surfaces, J. Phys.: Condens. Matter **18**, 7021 (2006).

[48] P. Söderlind, P. E. A. Turchi, A. Landa, and V. Lordi, Ground-state properties of rare-earth metals: An evaluation of density-functional theory, J. Phys.: Condens. Matter **26**, 416001 (2014).

[49] Y. Lee, R. Skomski, X. Wang, P. P. Orth, A. K. Pathak, B. N. Harmon, R. J. McQueeney, I. I. Mazin, and L. Ke, Interplay between magnetism and band topology in Kagome magnets $R\mathrm{Mn}_6\mathrm{Sn}_6$, arXiv:2201.11265.

[50] Y. Shao, A. N. Rudenko, J. Hu, Z. Sun, Y. Zhu, S. Moon, A. J. Millis, S. Yuan, A. I. Lichtenstein, D. Smirnov, Z. Q. Mao, M. I. Katsnelson, and D. N. Basov, Electronic correlations in nodal-line semimetals, Nat. Phys. **16**, 636 (2020).

[51] M. M. Qazilbash, J. J. Hamlin, R. E. Baumbach, L. Zhang, D. J. Singh, M. B. Maple, and D. N. Basov, Electronic correlations in the iron pnictides, Nat. Phys. **5**, 647 (2009).

[52] S. Fratini, S. Ciuchi, and D. Mayou, Phenomenological model for charge dynamics and optical response of disordered systems: Application to organic semiconductors, Phys. Rev. B **89**, 235201 (2014).

[53] J. P. Perdew, K. Burke, and M. Ernzerhof, Generalized Gradient Approximation Made Simple, Phys. Rev. Lett. **77**, 3865 (1996).

[54] P. Blaha, K. Schwarz, G. Madsen, D. Kvasnicka, J. Luitz, R. Laskowski, F. Tran, and L. Marks, *WIEN2k, An Augmented Plane Wave + Local Orbitals Program for Calculating Crystal Properties* (Karlheinz Schwarz, Technische Universität Wien, Austria, 2018).

[55] Q. Wang, K. J. Neubauer, C. Duan, Q. Yin, S. Fujitsu, H. Hosono, F. Ye, R. Zhang, S. Chi, K. Krycka, H. Lei, and P. Dai, Field-induced topological Hall effect and double-fan spin structure with a *c*-axis component in the metallic kagome antiferromagnetic compound $\mathrm{YMn}_6\mathrm{Sn}_6$, Phys. Rev. B **103**, 014416 (2021).

[56] D. Gorbunov, M. Kuz'min, K. Uhlířová, M. Žáček, M. Richter, Y. Skourski, and A. Andreev, Magnetic properties of a $\mathrm{GdMn}_6\mathrm{Sn}_6$ single crystal, J. Alloys Compd. **519**, 47 (2012).

[57] C. C. Homes, M. Reedyk, D. A. Cradles, and T. Timusk, Technique for measuring the reflectance of irregular, submillimeter-sized samples, Appl. Opt. **32**, 2976 (1993).

[58] D. B. Tanner, Use of x-ray scattering functions in Kramers-Kronig analysis of reflectance, Phys. Rev. B **91**, 035123 (2015).

[59] G. Kresse and J. Furthmüller, Efficiency of *ab-initio* total energy calculations for metals and semiconductors using a plane-wave basis set, Comput. Mater. Sci. **6**, 15 (1996).

[60] G. Kresse and J. Furthmüller, Efficient iterative schemes for *ab initio* total-energy calculations using a plane-wave basis set, Phys. Rev. B **54**, 11169 (1996).

[61] C. Ambrosch-Draxl and J. Sofo, Linear optical properties of solids within the full-potential linearized augmented planewave method, Comput. Phys. Commun. **175**, 1 (2006).